AJR Online First Accepted Manuscript

Liver Steatosis Categorization on Contrast-Enhanced CT Using a Fully-Automated Deep Learning Volumetric Segmentation Tool: Evaluation in 1,204 Heathy Adults Using Unenhanced CT as Reference Standard

Perry J. Pickhardt, MD, Glen Blake, PhD, Peter M. Graffy, BA, Veit Sandfort, MD, Daniel C. Elton, PhD, Alberto A. Perez, BE, Ronald M. Summers, MD, PhD

doi:10.2214/AJR.20.24415
Accepted: August 25, 2020

The complete title page, as provided by the authors, is available at the end of this article.

Abstract

Background: Hepatic attenuation at unenhanced CT is linearly correlated with MR proton density fat fraction (PDFF). Liver fat quantification at contrast-enhanced CT is more challenging.

Objective: To evaluate liver steatosis categorization on contrast-enhanced CT using a fully-automated deep learning volumetric hepatosplenic segmentation algorithm and unenhanced CT as the reference standard.

Materials and Methods: A fully-automated volumetric hepatosplenic segmentation algorithm using 3D convolutional neural networks was applied to unenhanced and contrast-enhanced series from a sample of 1204 healthy adults (mean age, 45.2 years; 726 women, 478 men) undergoing CT evaluation for renal donation. The mean volumetric attenuation was computed from all designated liver and spleen voxels. PDFF was estimated from unenhanced CT attenuation and served as the reference standard. Contrast-enhanced attenuations were evaluated for detecting PDFF thresholds of 5% (mild steatosis), 10%, and 15% (moderate); PDFF<5% was considered normal.

Results: Using unenhanced CT as reference, estimated PDFF was ≥5% (mild steatosis), ≥10%, and ≥15% (moderate) in 50.1% (n=603), 12.5% (n=151) and 4.8% (n=58) of patients, respectively. ROC-AUC values for predicting PDFF thresholds of 5%, 10%, and 15% using contrast-enhanced liver attenuation were 0.669, 0.854, and 0.962, respectively, and using contrast-enhanced liver-spleen attenuation difference were 0.662, 0.866, and 0.986, respectively. A total of 96.8% (90/93) of patients with contrast-enhanced liver attenuation <90 HU had steatosis (PDFF≥5%); this <90 HU threshold achieved sensitivity 75.9% and specificity 95.7% for moderate steatosis (PDFF≥15%). Liver attenuation <100 HU achieved sensitivity 34.0% and specificity 94.2% for any steatosis (PDFF≥5%). A total of 93.8% (30/32) of patients with contrast-enhanced liver-spleen attenuation difference <-10 HU had moderate steatosis (PDFF≥15%); a liver-spleen difference <5 HU achieved sensitivity 91.4% and specificity 95.0% for moderate steatosis. Liver-spleen difference <10 HU achieved sensitivity 29.5% and specificity 95.5% for any steatosis (PDFF≥5%).

Conclusion: Contrast-enhanced volumetric hepatosplenic attenuation derived using a fully-automated deep-learning CT tool may allow objective categorical assessment of hepatic steatosis. Accuracy was better for moderate than mild steatosis. Further confirmation using different scanning protocols and vendors is warranted.

Clinical Impact: If these results are confirmed in independent patient samples, this automated approach could prove useful for both individualized and population-based steatosis assessment.

Recommended citation:
Pickhardt PJ, Blake G, Graffy PM, Sandfort V, Elton DC, Perez AA, Summers RM. Liver Steatosis Categorization on Contrast-Enhanced CT Using a Fully-Automated Deep Learning Volumetric Segmentation Tool: Evaluation in 1,204 Heathy Adults Using Unenhanced CT as Reference Standard. *AJR* September 16, 2020. Accepted manuscript. doi:10.2214/AJR.20.24415

Highlights:

Key Finding: Using estimated MR proton density fat fraction (PDFF) from unenhanced CT as reference, contrast-enhanced liver attenuation from a fully-automated deep learning volumetric segmentation tool achieved ROC-AUC of 0.962 for detecting moderate steatosis (PDFF≥15%), as well as sensitivity 75.9% and specificity 95.7% at a contrast-enhanced CT threshold of <90 HU threshold.

Importance: Opportunistic detection of hepatic steatosis on abdominal CT performed for other indications may help address non-alcoholic fatty liver disease, a highly prevalent public health issue.

Introduction

Non-alcoholic fatty liver disease (NAFLD) is a highly prevalent public health issue, with cardiovascular, metabolic, and liver-specific implications. [1-3] Although not a defining criterion, NAFLD is closely associated with the obesity and metabolic syndrome epidemics that are prevalent throughout the world.[4-6] A majority of American adults are now considered obese, and approximately half of all American adults may have some degree of hepatic steatosis. [7,8] Despite its growing importance, there is no reliable non-invasive, non-imaging based clinical method for accurately quantifying or even categorizing the degree of steatosis. Liver biopsy for the sole purpose of assessing hepatic steatosis at histopathology is costly and invasive, and generally provides only a subjective visual estimate of steatosis, in addition to sampling error. From a population-based standpoint, non-invasive imaging methods for liver fat quantification appear advantageous.

MRI proton density fat fraction (PDFF) should be the preferred non-invasive reference standard for quantifying liver fat given its accuracy and whole-liver assessment.[9] Recent studies using different CT vendors demonstrated the linear equivalence between MR-PDFF and unenhanced CT attenuation [10-12]. This equivalence allows CT to be used to quantify liver fat, especially beyond normal or low levels. Furthermore, because abdominal CT is obtained in clinical practice much more frequently than abdominal MRI, CT can serve as a surrogate for initial detection of steatosis.[13] For these reasons, non-contrast CT may represent a practical non-invasive reference standards for routine liver fat quantification, especially for population-based studies.[14] However, CT assessment of liver fat content after IV contrast administration remains much more challenging.

A fully-automated algorithm for quantifying liver fat at unenhanced CT was recently validated in a large sample of patients without symptoms.[15] This volumetric deep learning tool was compared against the standard manual region-of-interest (ROI) approach.[11,16-18] The tool automatically segments and analyzes both the liver and spleen. However, to realize the full potential of this automated tool for

population-based opportunistic hepatic steatosis and NAFLD screening, the next challenge is to apply it to contrast-enhanced CT obtained in the portal venous phase or later. Although the direct linear relationship between CT attenuation and MR-based PDFF no longer holds following IV contrast administration, patients may potentially be placed into PDFF categories (eg, normal, mild steatosis, and moderate or greater steatosis) based on contrast-enhanced liver attenuation, with or without incorporating splenic attenuation. The purpose of this study was to evaluate liver steatosis categorization on contrast-enhanced CT using the fully-automated deep learning volumetric hepatosplenic segmentation algorithm and unenhanced CT as the reference standard.

Materials and Methods

Study Sample

This retrospective study was IRB-approved and HIPAA-compliant; the requirement for written informed consent was waived. A total of 1250 consecutive adults who underwent multiphasic abdominal CT at a single academic medical center for the purpose of potential renal donation between February 2010 and January 2017 were initially included. After exclusion of 46 patients due to missing or corrupted CT image data (n=39), or splenic absence (n=7), the final study sample consisted of 1204 healthy adults with usable CT image data. Prior to automated CT-based assessment, patient information was anonymized.

CT Protocol

All individuals in the study sample underwent abdominal CT using a dedicated multi-phasic protocol. All scans were performed on multi-detector-row CT scanners (GE Healthcare, Waukesha, WI) predominately employing a size-based protocol with 64 x 0.625 detector configuration, 120 kV_p, modulated mA, and noise index ranging from 17.0-27.5. A pre-contrast abdominal series was obtained extending from T12-L4. A split-bolus IV contrast technique was used to achieve multi-phase dynamic and excretory imaging. An initial injection consisted of 20 ml of nonionic contrast (with 20 ml saline flush) five minutes prior to the dynamic multi-phasic injection to opacify the upper collecting system. Dynamic multi-phasic injection consisted of split bolus of 30 ml contrast (and 30 ml saline) at 3 ml/second for the arterial (vascular) phase, followed by 100 ml contrast/50 ml saline at 5 ml/second twenty seconds later for the late portal venous (parenchymal) phase. Arterial and parenchymal phase series were then obtained. The arterial phase was intended for renal vascular assessment and did not provide sufficient hepatic coverage for the present investigation. The arterial phase is also of less

practical value for liver fat quantification given this phase's greater sensitivity to timing and hypervascularity of the spleen. Thus, this study used only the unenhanced and parenchymal contrast-enhanced phases for assessing the automated CT tool. Imaging series were originally reconstructed as 5 mm slices at 3-mm intervals, which were then retrospectively reformatted to 3-mm contiguous slices.

Automated Algorithm for Hepatosplenic Segmentation and Analysis

The methodology for automated hepatosplenic assessment has been previously described in detail.[19] A modified 3D U-Net was employed. Imaging data for training were obtained from a separate patient sample.[20] Data augmentation was performed using 3D rotation, crop, elastic deformation, CycleGAN for the non-contrast images, and random flips. Training of the model used the NIH Biowulf HPC cluster. The volumetric meanattenuation was computed for all designated liver voxels. The intrahepatic vasculature was included in the segmentation. A similar process was used for the spleen.

Liver Fat Quantification Reference Standard

The mean unenhanced CT liver attenuation obtained from the automated volumetric tool was converted to the MR-based PDFF equivalent fat fraction using the recently published formula: *Fat fraction (%) = -0.58(CT HU) + 38.2*.[11] This unenhanced CT hepatic fat fraction served as the reference standard to which the contrast-enhanced attenuation was compared. The linear relationship between CT hepatic fat fraction and PDFF equivalent has been verified in a prospective trial using a different CT vendor.[12] While various steatosis categories according to PDFF have been used, a recent study suggests that 5% should serve as the preferred threshold for normal (<5%) versus mild steatosis, and 15% as the preferred threshold between mild and moderate steatosis.[21] We adopted these fat fraction thresholds of 5% and 15%, and used 10% to signify the midway point between mild and moderate steatosis. Although the prevalence of fat fraction >20% was expected to be low in a sample of healthy outpatients, we considered this to signify a relatively more severe degree of steatosis.

Statistical Analysis

Sensitivity, specificity, positive predictive values (PPV), negative predictive values (NPV) and receiver operating characteristic (ROC) curves for PDFF thresholds of 5%, 10% and 15% were calculated in Excel spreadsheets. Starting from columns of unenhanced and contrast-enhanced liver attenuations,

the unenhanced attenuations were first converted to MR-PDFF equivalent fat fractions using the calibration formula cited above. Each case was then identified as positive or negative for steatosis according to the selected PDFF thresholds (5%, 10% or 15%). For each threshold, true positive (TP), true negative (TN), false positive (FP), and false negative (FN) results were determined to derive sensitivity, specificity, PPV, NPV, and ROC curves. The area under each ROC curve (AUC) was derived by summing all 1204 elemental areas individually calculated using the trapezoid method.[22] The statistical significance of the difference between the AUCs for enhanced CT liver attenuation and enhanced CT liver–spleen attenuation difference at each PDFF threshold was evaluated using the method of Hanley & McNeil.[23]

Results

The mean age (± SD) of the 1204 healthy adults was 45.2 ± 12.4 years. The sample included 478 men and 726 women. Based on the unenhanced CT reference standard and the PDFF conversion formula (-0.58(CT HU) + 38.2), the corresponding PDFF indicated ≥5% (mild) steatosis in 50.1% (603/1204), ≥10% steatosis in 12.5% (151/1204), ≥15% (moderate) steatosis in 4.8% (58/1204), and ≥20% steatosis in 1.4% (17/1204).

The automated tool was successful run and provided a measure in all 1204 cases. Figure 1 demonstrates scatterplots for both contrast-enhanced liver attenuation and liver-spleen attenuation difference versus PDFF (derived from the unenhanced liver attenuation). Prediction performance improved with greater degrees of underlying hepatic steatosis. ROC AUC values for automated contrast-enhanced liver attenuation alone in predicting PDFF thresholds of 5%, 10%, and 15% were 0.669, 0.854, and 0.962, respectively (Fig 2A). ROC AUC values for contrast-enhanced liver-spleen attenuation difference in predicting PDFF thresholds of 5%, 10%, and 15% were 0.669, 0.854, and 0.962, respectively (Fig 2B). These ROC AUC values were not significantly different between the two measures (p=0.66, 0.54, and 0.19, respectively).

Figure 3 depicts bar graphs of PDFF or steatosis categories for a variety of contrast-enhanced liver attenuation thresholds and ranges. A total of 96.8% (90/93) of patients with a contrast-enhanced liver attenuation <90 HU had PDFF≥5% (at least mild steatosis). A total of 96.8% (727/751) of patients with a contrast-enhanced liver attenuation >110 HU had PDFF<10%. Table 1 provides more detailed performance data for predicting steatosis categories according to relevant contrast-enhanced liver attenuation thresholds. For example, to predict moderate steatosis (PDFF>15%), a contrast-enhanced threshold of <90 HU achieved sensitivity 75.9%, specificity 95.7%, PPV 47.3%, and NPV 98.7%. To predict

moderate steatosis, increasing the CT threshold to 110 HU achieved higher sensitivity of 98.3%, though decreased specificity of 65.5%, while decreasing the CT threshold to 80 HU achieved higher specificity of 99.2%, though decreased sensitivity of 55.2%. To predict any degree of hepatic steatosis (PDFF >5%), a contrast-enhanced threshold <120 HU achieved sensitivity 74.7% and specificity 52.1%; <100 HU achieved sensitivity 34.0% and 94.2%; and <80 HU achieved sensitivity 6.8% and specificity 100.0%.

Figure 4 depicts bar graphs of PDFF or steatosis categories for a variety of contrast-enhanced liver-spleen HU difference thresholds and ranges. A total of 93.8% (30/32) of patients with a liver-spleen difference of <-10 HU had PDFF≥15% (at least moderate steatosis). A total of 100.0% (15/15) of patients with a liver-spleen attenuation difference of <-20 HU had PDF≥15%. A total of 86.8% (178/205) of patients with a liver-spleen attenuation difference of <10 HU had PDFF≥5% (at least mild steatosis). Table 2 provides more detailed performance data for predicting steatosis categories according to relevant contrast-enhanced liver-spleen attenuation difference thresholds. For example, to predict moderate steatosis (PDFF>15%), a contrast-enhanced liver-spleen attenuation difference threshold of <5 HU achieved sensitivity 91.4%, specificity 95.0%, PPV 48.2%, and NPV 99.5%. To predict any degree of hepatic steatosis (PDFF>5%), a contrast-enhanced liver-spleen attenuation difference of <10 HU achieved sensitivity 29.5% and specificity 95.5%, and <0 HU (i.e., liver attenuation less than that of the spleen) achieved sensitivity 1.8% and specificity 100.0%.

Discussion

Although it has been demonstrated that liver fat content can be directly estimated on unenhanced CT scans using the linear conversion formula with MR-based PDFF,[10,11] quantification at contrast-enhanced CT remains elusive, owing to the complexities of hepatic contrast enhancement. Nonetheless, we found that categorical assignment of fat content based on contrast-enhanced CT is feasible, especially for at least moderate steatosis. Using the contrast-enhanced liver attenuation alone performed well and is more straightforward than including splenic attenuation. As such, our data do not clearly support the inclusion of splenic attenuation. Regardless, distinction between normal and mild steatosis (ie, around the 5% PDFF threshold) remains a diagnostic challenge using contrast-enhanced CT attenuation given very low sensitivity. External validation of our findings in a variety of practice settings is still needed.

The ability to use unenhanced CT as the reference standard for liver fat content was advantageous. Put in context for routine practice, the unenhanced CT thresholds for any steatosis (PDFF

≥5%) and moderate steatosis (PDFF ≥15%) correspond to 57 HU and 40 HU, respectively, at 120 kV_p. However, on clinical patient scans, the relationship between unenhanced CT attenuation and MR-PDFF weakens somewhat at lower levels of fat content (eg, ~5% PDFF) compared with performance in a phantom model.[11,12] Earlier work also showed lower agreement between unenhanced CT and histopathology near the threshold between normal and mild steatosis.[24] This may help explain why contrast-enhanced CT performance in our study was poorer around the 5% PDFF threshold. While splenic attenuation provides no additional value to liver attenuation for liver fat quantification at unenhanced CT,[16,25] it has shown variable utility after IV contrast, expressed either as a ratio or difference with liver attenuation.[26-28]

Other investigators have also studied the ability of contrast-enhanced hepatosplenic attenuation to predict hepatic steatosis,[26-28] typically with manual ROI technique and a histopathologic reference standard. As with our findings, the results are generally reported in categorical terms (eg, normal versus mild or moderate steatosis) and not as a continuous percentage. One study found that a liver-spleen attenuation difference of -19 HU was the optimal cut-off for moderate steatosis, as defined by ≥30% lipid droplets at histopathology.[26] However, another study showed that the absolute contrast-enhanced liver attenuation alone performed better than the liver attenuation normalized to spleen, either by an absolute difference or ratio.[27] Yet another study found that the rate and timing of contrast injection significantly influenced the optimal liver-spleen attenuation threshold for diagnosing fatty liver.[28]

Dual-energy CT (DECT) offers another potential solution to quantifying liver fat at contrast-enhanced CT. As with splenic attenuation assessment, DECT does not improve upon unenhanced single-energy CT for liver fat quantification,[10,29] except potentially in cases of superimposed iron overload or amiodarone therapy.[30-32] However, in the setting of iodinated contrast material, a multi-material decomposition approach has provided direct liver fat quantification in experimental studies.[32,33] A more simplistic clinical DECT approach consists of deriving virtual non-contrast (VNC) images that, if closely matched to true non-contrast liver attenuation, would provide fat quantification. In practice, however, the fidelity of VNC matching with the true non-contrast HU values can vary according to scanner vendor and model.[34,35]

Whether cause or effect, NAFLD is related to diabetes, obesity, hyperlipidemia, and metabolic syndrome.[6] The presence of at least mild steatosis (PDFF >5%) is remarkably common among adults in the U.S. and other industrialized populations, and is a largely asymptomatic condition. The 50% prevalence of hepatic steatosis in our sample of healthy adults undergoing potential renal donation is similar to the prevalence of 52% in a recent study of over 10,000 CT colonography examinations in

healthy adults undergoing colorectal cancer screening.[8] That prior sample, which was older on average (mean age 57 years, vs 45 years for the current sample) did show a higher prevalence of moderate or severe steatosis (10% based on PDFF≥14%) compared with our current sample (5% based on PDFF≥15%). The prevalence of hepatic steatosis is lower, typically around 20-25%, when estimated using liver enzyme elevation or ultrasound rather than CT.[36]

A recent study found a weak correlation between hepatic steatosis and BMI,[8] which implies that fatty liver cannot be reliably inferred from body habitus. Although hepatic and visceral fat are not defining criteria for metabolic syndrome, they appear to provide valuable information beyond BMI,[5] and may ultimately provide an improved definition of metabolic syndrome.[6] Another recent study showed that automated CT-based assessment of hepatic steatosis was predictive of future adverse events, including major cardiovascular events and mortality.[37] Automated CT-based assessment of these key abdominal fat measures could be used for opportunistic NAFLD and metabolic syndrome screening, regardless of the reason for the scan.

Large volumes of abdominal CT are performed each year,[13] presenting an opportunity to screen for many conditions beyond the primary imaging indication. In addition to hepatic steatosis,[16-18] CT can also non-invasively evaluate the liver for fibrosis[38-42] and hemochromatosis.[30] Beyond the liver and metabolic syndrome, other opportunistic screening examples include osteoporosis and associated fractures, abdominal aortic calcification and aneurysm, sarcopenia, and cancer.[43-47] Many of these opportunistic tasks can be automated through AI,[48] avoiding the subjectivity and time constraints related to manual measurements.

We acknowledge limitations to this investigation. All scans were derived from a single academic institution employing scanners from a single CT vendor. The contrast-enhanced phase used in this study was not a pure portal venous acquisition. However, the scanning protocol ensured adequate timing for liver parenchymal enhancement, whereas the portal venous phase can be obtained too early in some patients. Nonetheless, further external validation of this automated tool is warranted in diverse patient populations, with additional scanning protocols including a true portal venous phase, and with other CT vendors. Our reference standard for liver fat quantification was based on unenhanced CT, for which a previously validated formula was used to convert to an MR-based PDFF equivalent. This approach may also warrant validation in a wider variety of practice settings. However, advantages over histopathologic correlation of using MR-based PDFF, and by extension unenhanced CT, as reference standard include its precision, objectivity, wider sampling, and non-invasiveness. Finally, inclusion of intrahepatic vessels in the automated liver segmentation may affect liver attenuation estimation. For

unenhanced CT, this may partially explain the mean 2.7 attenuation difference between manual and automated techniques.[8] For contrast-enhanced CT, the impact of vessel inclusion should be greater with higher degrees of steatosis, given a more pronounced difference between enhanced vessel and parenchyma. Nonetheless, we believe the impact of vessel inclusion to be very small.

In conclusion, contrast-enhanced hepatic and splenic attenuation derived using a fully-automated deep learning volumetric segmentation CT tool allowed for adequate categorical assessment of hepatic steatosis, especially at higher PDFF levels. The contrast-enhanced liver attenuation alone performed reasonably well, potentially precluding the need for splenic attenuation consideration. This automated approach could prove useful for both individualized and population-based assessments for NALFD if our findings are confirmed by other groups.

References

1. Lonardo A, Ballestri S, Marchesini G, Angulo P, Loria P. Nonalcoholic fatty liver disease: a precursor of the metabolic syndrome. Dig Liver Dis 2015;47:181.
2. Targher G, Byrne CD, Lonardo A, Zoppini G, Barbui C. Non-alcoholic fatty liver disease and risk of incident cardiovascular disease: a meta-analysis. J Hepatol 2016;65:589.
3. Wree A, Broderick L, Canbay A, Hoffman HM, Feldstein AE. From NAFLD to NASH to cirrhosis—new insights into disease mechanisms. Nat Rev Gastroenterol Hepatol 2013;10:627.
4. Neeland IJ, Ross R, Despres JP, et al. Visceral and ectopic fat, atherosclerosis, and cardiometabolic disease: a position statement. The lancet Diabetes & endocrinology 2019;7:715-25.
5. Pickhardt PJ, Jee Y, O'Connor SD, Munoz del Rio A. Visceral adiposity and hepatic steatosis at abdominal CT: association with the metabolic syndrome. American Journal of Roentgenology 2012;198:1100-7.
6. Pickhardt PJ, Graffy PM, Zea R, et al. Opportunistic Screening for Metabolic Syndrome in Asymptomatic Adults Utilizing Fully Automated Abdominal CT-based Biomarkers. AJR Am J Roentgenol 2020.
7. Bellentani S. The epidemiology of non-alcoholic fatty liver disease. Liver international : official journal of the International Association for the Study of the Liver 2017;37 Suppl 1:81-4.
8. Graffy PM, Sandfort V, Summers RM, Pickhardt PJ. Automated Liver Fat Quantification at Nonenhanced Abdominal CT for Population-based Steatosis Assessment. Radiology 2019;293:334-42.
9. Reeder SB, Hu HH, Sirlin CB. Proton density fat-fraction: a standardized MR-based biomarker of tissue fat concentration. J Magn Reson Imaging 2012;36:1011.
10. Kramer H, Pickhardt PJ, Kliewer MA, et al. Accuracy of Liver Fat Quantification With Advanced CT, MRI, and Ultrasound Techniques: Prospective Comparison With MR Spectroscopy. American Journal of Roentgenology 2017;208:92-100.
11. Pickhardt PJ, Graffy PM, Reeder SB, Hernando D, Li K. Quantification of Liver Fat Content With Unenhanced MDCT: Phantom and Clinical Correlation With MRI Proton Density Fat Fraction. AJR Am J Roentgenol 2018;211:W151-W7.
12. Guo Z, Blake GM, Li K, et al. Liver Fat Content Measurement with Quantitative CT Validated against MRI Proton Density Fat Fraction: A Prospective Study of 400 Healthy Volunteers. Radiology 2020;294:89-97.
13. Moreno CC, Hemingway J, Johnson AC, Hughes DR, Mittal PK, Duszak R. Changing Abdominal Imaging Utilization Patterns: Perspectives From Medicare Beneficiaries Over Two Decades. J Am Coll Radiol 2016;13:894-903.
14. Starekova J, Hernando D, Pickhardt PJ, Reeder SB. Quantification of liver fat content with CT and MRI: state of the art. Radiology (submitted).
15. Graffy PM, Sandfort V, Summers RM, Pickhardt PJ. Automated Liver Fat Quantification at Nonenhanced Abdominal CT for Population-based Steatosis Assessment. Radiology 2019:190512.
16. Boyce CJ, Pickhardt PJ, Kim DH, et al. Hepatic Steatosis (Fatty Liver Disease) in Asymptomatic Adults Identified by Unenhanced Low-Dose CT. American Journal of Roentgenology 2010;194:623-8.
17. Hahn L, Reeder SB, Del Rio AM, Pickhardt PJ. Longitudinal Changes in Liver Fat Content in Asymptomatic Adults: Hepatic Attenuation on Unenhanced CT as an Imaging Biomarker for Steatosis. AJR Am J Roentgenol 2015;205:1167-72.
18. Pickhardt PJ, Hahn L, del Rio AM, Park SH, Reeder SB, Said A. Natural History of Hepatic Steatosis: Observed Outcomes for Subsequent Liver and Cardiovascular Complications. American Journal of Roentgenology 2014;202:752-8.

19. Sandfort V, Yan K, Pickhardt PJ, Summers RM. Data augmentation using generative adversarial networks (CycleGAN) to improve generalizability in CT segmentation tasks. Sci Rep 2019;9:16884.
20. Simpson AL, Antonelli M, Bakas S, et al. A large annotated medical image dataset for the development and evaluation of segmentation algorithms. arXiv preprint arXiv:190209063 2019.
21. Cunha GM, Thai TT, Hamilton G, et al. Accuracy of common proton density fat fraction thresholds for magnitude- and complex-based chemical shift-encoded MRI for assessing hepatic steatosis in patients with obesity. Abdominal radiology (New York) 2020;45:661-71.
22. Delong ER, Delong DM, Clarkepearson DI. COMPARING THE AREAS UNDER 2 OR MORE CORRELATED RECEIVER OPERATING CHARACTERISTIC CURVES - A NONPARAMETRIC APPROACH. Biometrics 1988;44:837-45.
23. Hanley JA, McNeil BJ. A METHOD OF COMPARING THE AREAS UNDER RECEIVER OPERATING CHARACTERISTIC CURVES DERIVED FROM THE SAME CASES. Radiology 1983;148:839-43.
24. Lee SS, Park SH, Kim HJ, et al. Non-invasive assessment of hepatic steatosis: prospective comparison of the accuracy of imaging examinations. J Hepatol 2010;52:579-85.
25. Pickhardt PJ, Park SH, Hahn L, Lee S-G, Bae KT, Yu ES. Specificity of unenhanced CT for non-invasive diagnosis of hepatic steatosis: implications for the investigation of the natural history of incidental steatosis. European Radiology 2012;22:1075-82.
26. Kim DY, Park SH, Lee SS, et al. Contrast-enhanced computed tomography for the diagnosis of fatty liver: prospective study with same-day biopsy used as the reference standard. Eur Radiol 2010;20:359-66.
27. Kodama Y, Ng CS, Wu TT, et al. Comparison of CT methods for determining the fat content of the liver. AJR Am J Roentgenol 2007;188:1307-12.
28. Johnston RJ, Stamm ER, Lewin JM, Hendrick RE, Archer PG. Diagnosis of fatty infiltration of the liver on contrast enhanced CT: limitations of liver-minus-spleen attenuation difference measurements. Abdom Imaging 1998;23:409-15.
29. Artz NS, Hines CD, Brunner ST, et al. Quantification of Hepatic Steatosis With Dual-Energy Computed Tomography: Comparison With Tissue Reference Standards and Quantitative Magnetic Resonance Imaging in the ob/ob Mouse. Invest Radiol 2012;47:603-10.
30. Lawrence EM, Pooler BD, Pickhardt PJ. Opportunistic Screening for Hereditary Hemochromatosis With Unenhanced CT: Determination of an Optimal Liver Attenuation Threshold. American Journal of Roentgenology 2018;211:1206-11.
31. Laukamp KR, Lennartz S, Hashmi A, et al. Iodine accumulation of the liver in patients treated with amiodarone can be unmasked using material decomposition from multiphase spectral-detector CT. Scientific reports 2020;10:6994.
32. Fischer MA, Gnannt R, Raptis D, et al. Quantification of liver fat in the presence of iron and iodine: an ex-vivo dual-energy CT study. Invest Radiol 2011;46:351-8.
33. Hyodo T, Hori M, Lamb P, et al. Multimaterial Decomposition Algorithm for the Quantification of Liver Fat Content by Using Fast-Kilovolt-Peak Switching Dual-Energy CT: Experimental Validation. Radiology 2017;282:381-9.
34. Javadi S, Elsherif S, Bhosale P, et al. Quantitative attenuation accuracy of virtual non-enhanced imaging compared to that of true non-enhanced imaging on dual-source dual-energy CT. Abdominal radiology (New York) 2020;45:1100-9.
35. Laukamp KR, Ho V, Obmann VC, et al. Virtual non-contrast for evaluation of liver parenchyma and vessels: results from 25 patients using multi-phase spectral-detector CT. Acta radiologica (Stockholm, Sweden : 1987) 2019:284185119893094.
36. Younossi Z, Anstee QM, Marietti M, et al. Global burden of NAFLD and NASH: trends, predictions, risk factors and prevention. Nature reviews Gastroenterology & hepatology 2018;15:11-20.

37. Pickhardt PJ, Graffy PM, Zea R, et al. Automated CT biomarkers for opportunistic prediction of future cardiovascular events and mortality in an asymptomatic screening population: a retrospective cohort study. Lancet Digit Health 2020;2:E192-E200.
38. Pickhardt PJ, Malecki K, Kloke J, Lubner MG. Accuracy of Liver Surface Nodularity Quantification on MDCT as a Noninvasive Biomarker for Staging Hepatic Fibrosis. Am J Roentgenol 2016;207:1194-9.
39. Pickhardt PJ, Malecki K, Hunt OF, et al. Hepatosplenic volumetric assessment at MDCT for staging liver fibrosis. European Radiology 2017;27:3060-8.
40. Lubner MG, Jones D, Kloke J, Said A, Pickhardt PJ. CT texture analysis of the liver for assessing hepatic fibrosis in patients with hepatitis C virus. The British journal of radiology 2018:20180153.
41. Lubner MG, Pickhardt PJ. Multidetector Computed Tomography for Retrospective, Noninvasive Staging of Liver Fibrosis. Gastroenterology clinics of North America 2018;47:569-84.
42. Pickhardt PJ, Graffy PM, Said A, et al. Multiparametric CT for Noninvasive Staging of Hepatitis C Virus-Related Liver Fibrosis: Correlation With the Histopathologic Fibrosis Score. AJR American journal of roentgenology 2019;212:547-53.
43. Graffy PM, Liu J, Pickhardt PJ, Burns JE, Yao J, Summers RM. Deep learning-based muscle segmentation and quantification at abdominal CT: application to a longitudinal adult screening cohort for sarcopenia assessment. The British journal of radiology 2019:20190327.
44. Jang S, Graffy PM, Ziemlewicz TJ, Lee SJ, Summers RM, Pickhardt PJ. Opportunistic Osteoporosis Screening at Routine Abdominal and Thoracic CT: Normative L1 Trabecular Attenuation Values in More than 20 000 Adults. Radiology 2019;291:360-7.
45. O'Connor SD, Graffy PM, Zea R, Pickhardt PJ. Does Nonenhanced CT-based Quantification of Abdominal Aortic Calcification Outperform the Framingham Risk Score in Predicting Cardiovascular Events in Asymptomatic Adults? Radiology 2019;290:108-15.
46. Pickhardt PJ, Lee SJ, Liu JM, et al. Population-based opportunistic osteoporosis screening: Validation of a fully automated CT tool for assessing longitudinal BMD changes. The British journal of radiology 2019;92.
47. Pickhardt PJ, Kim DH, Meiners RJ, et al. Colorectal and extracolonic cancers detected at screening CT colonography in 10,286 asymptomatic adults. Radiology 2010;255:83-8.
48. Pickhardt PJ, Graffy PM, Lubner MG, Summers RM. Opportunistic screening at abdominal CT using automated biomarkers: adding value beyond the clinical indication. RadioGraphics (submitted).

Tables

Table 1. Sensitivity, specificity, positive predictive value and negative predictive value for various thresholds of enhanced CT liver attenuation to predict liver fat content based on proton density fat fractions (PDFF) >5%, >10% and, >15%.

	PDFF > 5%				PDFF > 10%				PDFF > 15%			
Attenuation (HU)‡	Sens (%)	Spec (%)	PPV (%)	NPV (%)	Sens (%)	Spec (%)	PPV (%)	NPV (%)	Sens (%)	Spec (%)	PPV (%)	NPV (%)
80	6.8	100.0	100.0	51.7	25.8	99.8	95.1	90.4	55.2	99.2	78.1	97.8
90	14.9	99.5	96.8	53.8	44.4	97.5	72.0	92.4	75.9	95.7	47.3	98.7
95	22.7	98.3	93.2	55.9	56.3	94.1	57.8	93.8	87.9	91.6	34.7	99.3
100	34.0	94.2	85.4	58.7	70.2	87.3	44.2	95.3	96.6	83.9	23.3	99.8
105	42.0	87.4	76.9	60.0	77.5	79.9	35.6	96.1	96.6	76.2	17.0	99.8
110	50.9	75.7	67.8	60.6	84.1	69.0	28.0	96.8	98.3	65.5	12.6	99.9
115	58.2	64.6	62.2	60.6	88.1	59.1	23.6	97.2	98.3	55.8	10.1	99.8
120	64.7	52.1	57.5	59.5	90.7	48.5	20.2	97.3	98.3	45.8	8.4	99.8

† **Enhanced CT liver HU** based on automated volumetric deep-learning tool

PDFF: Proton density fat fraction (based on unenhanced CT equivalent); Sens: Sensitivity; Spec: Specificity; PPV: Positive predictive value; NPV: Negative predictive value.

Table 2. Sensitivity, specificity, positive predictive value, and negative predictive value for various thresholds of enhanced CT liver–spleen attenuation (absolute HU difference) to predict liver fat content based on proton density fat fractions (PDFF) >5%, >10% and, >15%.

	PDFF > 5%				PDFF > 10%				PDFF > 15%			
Attenuation (HU)‡	Sens (%)	Spec (%)	PPV (%)	NPV (%)	Sens (%)	Spec (%)	PPV (%)	NPV (%)	Sens (%)	Spec (%)	PPV (%)	NPV (%)
-10	5.3	100.0	100.0	51.3	21.2	100.0	100.0	89.9	51.7	99.8	93.8	97.6
-5	8.0	100.0	100.0	52.0	31.1	99.9	97.9	91.0	70.7	99.4	85.4	98.5
0	10.8	100.0	100.0	52.8	41.1	99.7	95.4	92.2	79.3	98.3	70.8	99.0
5	17.6	99.3	96.4	54.6	55.0	97.4	75.5	93.8	91.4	95.0	48.2	99.5
10	29.5	95.5	86.8	57.5	68.2	90.3	50.2	95.2	98.3	87.1	27.8	99.9
15	45.1	82.2	71.8	59.9	80.8	75.6	32.2	96.5	100.0	72.0	15.3	100.0
20	63.2	57.4	59.8	60.9	90.1	52.4	21.4	97.4	100.0	49.5	9.1	100.0

‡ HU = Enhanced CT liver–spleen absolute HU difference, based on automated volumetric deep-learning tool

PDFF: Proton density fat fraction (based on unenhanced CT equivalent); Sens: Sensitivity; Spec: Specificity; PPV: Positive predictive value; NPV: Negative predictive value.

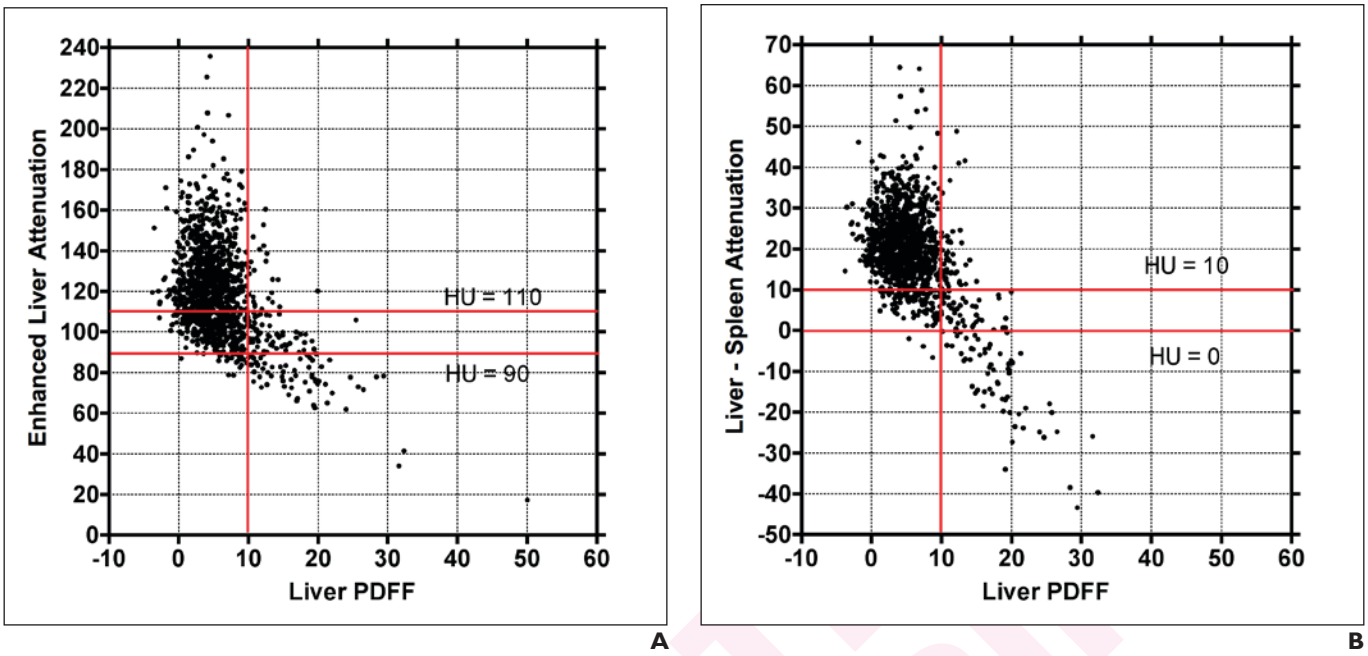

Figure 1. Scatterplots of enhanced CT (A) liver attenuation and (B) liver–spleen attenuation difference versus estimated MR proton density fat fraction (PDFF) based on the unenhanced CT series. The plots are similar for the two enhanced CT attenuation measures.

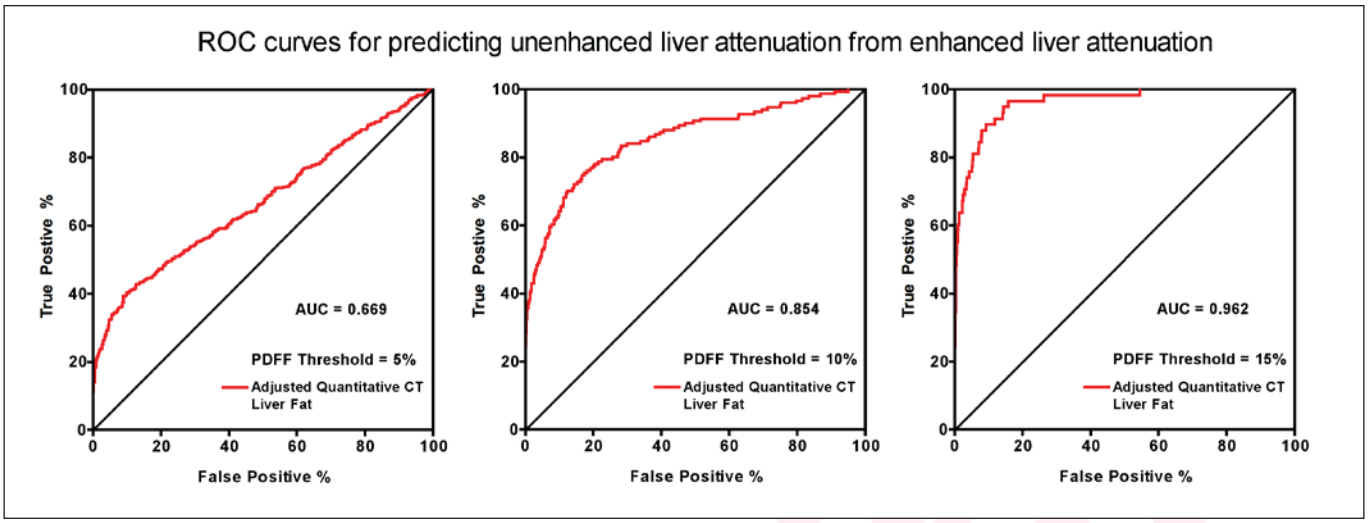

A

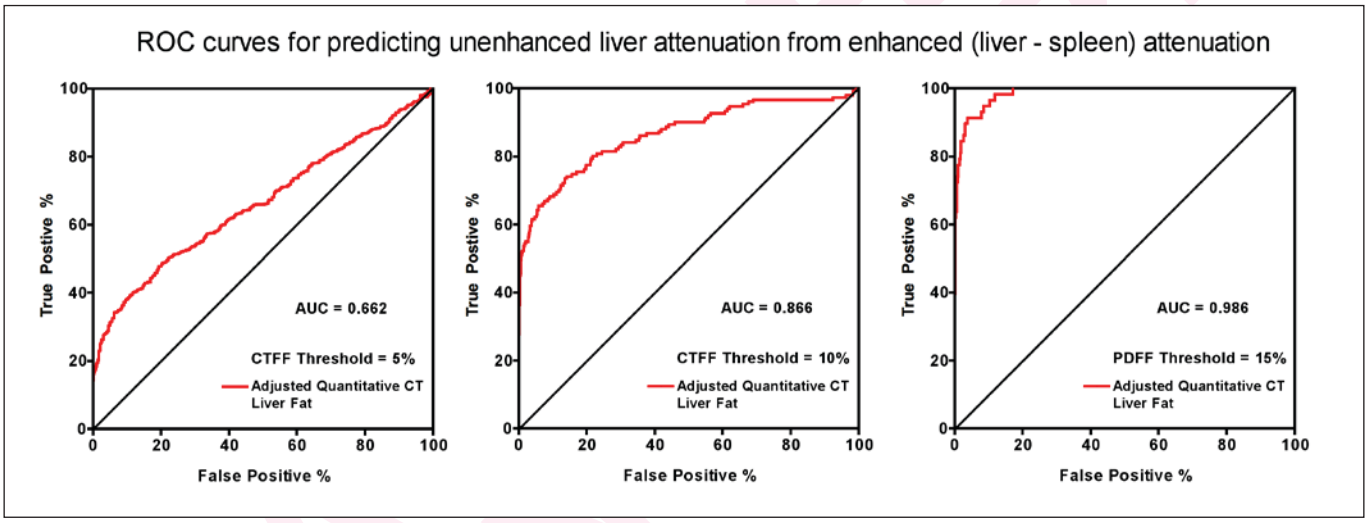

B

Figure 2. ROC curves for predicting liver fat content from the contrast-enhanced series. ROC curves are shown for PDFF-equivalent thresholds of 5% (left), 10% (middle), and 15% (right) for enhanced liver attenuation (A) and liver-spleen attenuation difference (B). The corresponding AUC values are similar for each of the three steatosis thresholds. Performance improves for greater degrees of steatosis.

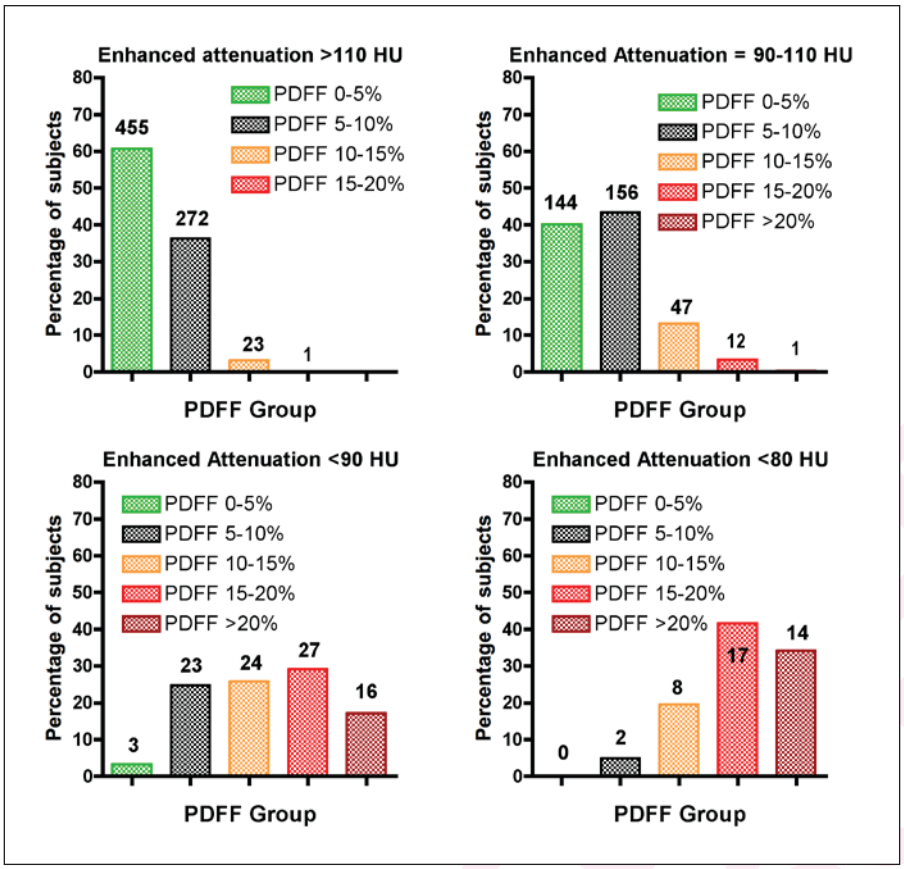

Figure 3. Bar graphs depicting liver fat content categories according to various thresholds and ranges for contrast-enhanced liver attenuation values.

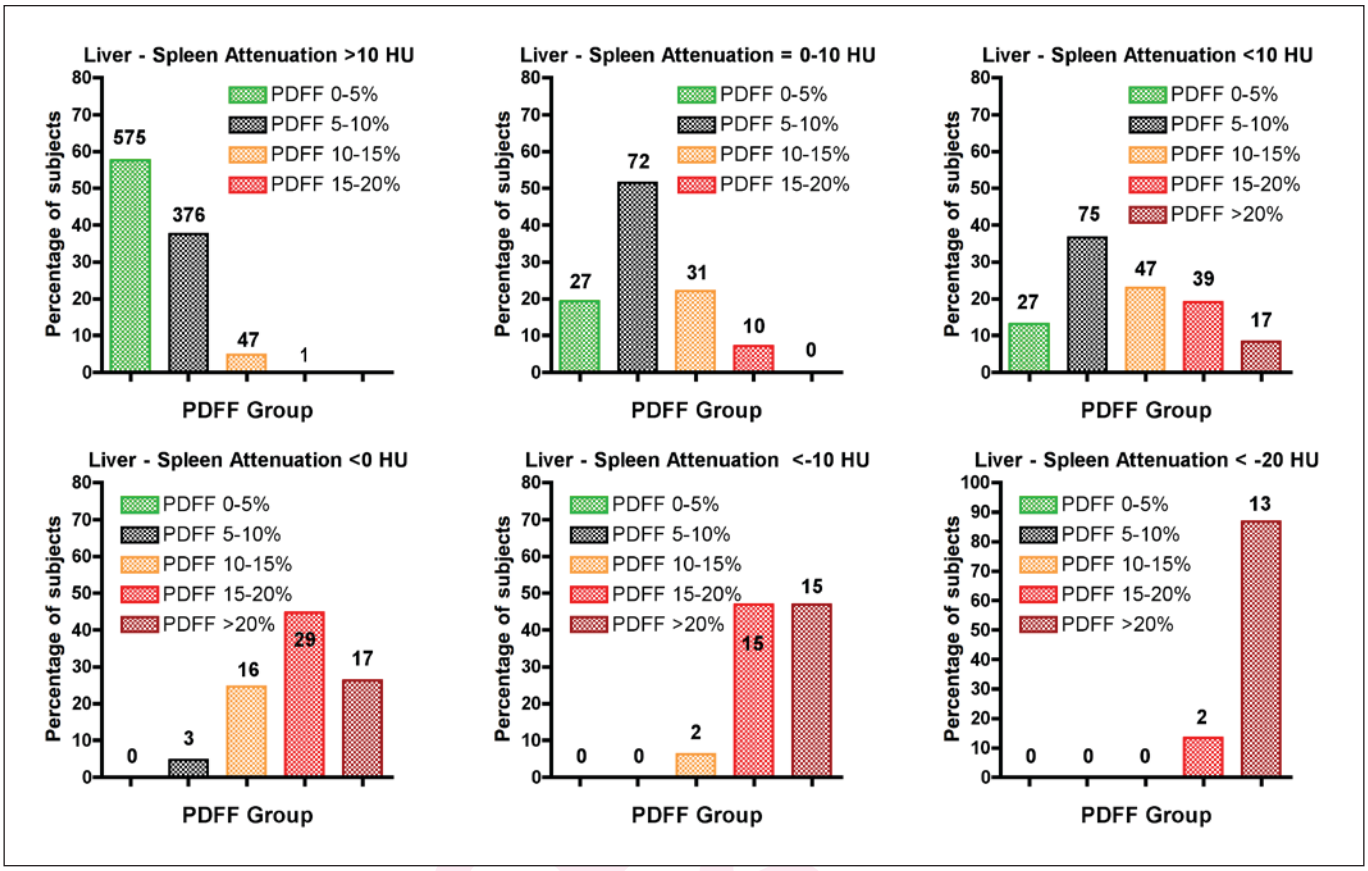

Figure 4. Bar graphs depicting liver fat content categories according to various thresholds and ranges for contrast-enhanced liver–spleen attenuation differences.

AJR

Liver Steatosis Categorization on Contrast-Enhanced CT Using a Fully-Automated Deep Learning Volumetric Segmentation Tool:

Evaluation in 1,204 Heathy Adults Using Unenhanced CT as Reference Standard

Original Research

Perry J. Pickhardt, MD[1]

Glen M Blake, PhD[2]

Peter M. Graffy, BA[1]

Veit Sandfort, MD[3]

Daniel C. Elton, PhD3

Alberto A. Perez, BE[1]

Ronald M. Summers, MD, PhD3

1. The University of Wisconsin School of Medicine & Public Health, Madison, WI
2. School of Biomedical Engineering & Imaging Sciences, King's College London, St Thomas' Hospital, London SE1 7EH, United Kingdom
3. Imaging Biomarkers and Computer-Aided Diagnosis Laboratory, Radiology and Imaging Sciences, National Institutes of Health Clinical Center, Bethesda, MD

Acknowledgments: This research was supported in part by the Intramural Research Program of the National Institutes of Health Clinical Center, and utilized the high performance computing capabilities of the NIH Biowulf cluster.
We thank NVIDIA for GPU card donation.

Disclosures: Dr. Pickhardt serves as an advisor to Bracco and Zebra and is a shareholder in SHINE, Elucent, and Cellectar; Dr. Summers receives royalties from iCAD, PingAn, Philips, ScanMed and Translation Holdings and research support from PingAn (CRADA) and NVIDIA (GPU card donations).

Corresponding author: Perry J. Pickhardt, MD
Department of Radiology
University of Wisconsin School of Medicine & Public Health
E3/311 Clinical Science Center
600 Highland Ave.
Madison, WI 53792-3252
e-mail: ppickhardt2@uwhealth.org
phone: 608-263-9028 fax: 608-263-0140